01 May 2019

Mechanical Properties of Heusler Alloys

Wesley Everhart

Joseph William Newkirk
Missouri University of Science and Technology, jnewkirk@mst.edu

Recommended Citation

W. Everhart and J. W. Newkirk, "Mechanical Properties of Heusler Alloys," *Heliyon*, vol. 5, no. 5, Elsevier Ltd, May 2019.
The definitive version is available at https://doi.org/10.1016/j.heliyon.2019.e01578

Heliyon 5 (2019) e01578

Contents lists available at ScienceDirect

Heliyon

journal homepage: www.heliyon.com

Heliyon

Review Article

Mechanical properties of Heusler alloys

Wesley Everhart [a,*], Joseph Newkirk [b]

[a] Kansas City National Security Campus, United States
[b] Missouri University of Science and Technology, United States

ARTICLE INFO

Keywords:
Metallurgical engineering
Materials science

ABSTRACT

Heusler alloys have been a significant topic of research due to their unique electronic structure, which exhibits half-metallicity, and a wide variety of properties such as magneto-calorics, thermoelectrics, and magnetic shape memory effects. As the maturity of these materials grows and commercial applications become more near-term, the mechanical properties of these materials become an important factor to both their processing as well as their final use. Very few studies have experimentally investigated mechanical properties, but those that exist are reviewed within the context of their magnetic performance and application space with specific focus on elastic properties, hardness and strength, and fracture toughness and ductility. A significant portion of research in Heusler alloys are theoretical in nature and many attempt to provide a basic view of elastic properties and distinguish between expectations of ductile or brittle behavior. While the ease of generating data through atomistic methods provides an opportunity for wide reaching comparison of various conceptual alloys, the lack of experimental validation may be leading to incorrect conclusions regarding their mechanical behavior. The observed disconnect between the few available experimental results and the numerous modeling results highlights the need for more experimental work in this area.

1. Introduction

Heusler alloys were originally discovered in 1903 and garnered interest due to the observed ferromagnetism without the presence of magnetic elements [1]. Soon after, the observance of half-metallic behavior began to drive significant research to develop and understand the nature of the combined semi-conducting and magnetic behavior leading to numerous new Heusler alloys. The wide variety of properties and the potential for tailoring the magnetic properties to the desired need have led to over 1000 publications on Heusler alloys since 2015.

Four main structural categories of Heusler alloys can be defined. Full-Heusler alloys (X_2YZ) such as Ni_2TiAl exhibit the $L2_1$ structure with $Fm\bar{3}m$ symmetry, which can be represented by four interpenetrating FCC lattices [1, 2]. The X and Y atoms are typically transition elements or lanthanides while the Z atom is from group III or IV. Heusler alloys exhibit Slater-Pauling behavior where the total magnetic moment is equal to the number of uncompensated electron spins [3]. Full-Heusler alloys exhibit such behavior where the total magnetic moment can typically be approximated with Eq. (1).

$$M_t = Z_t - 24 \tag{1}$$

Where M_t is the total magnetic moment, Z_t is the total number of valence electrons, and 24 is two times the number of minority band electrons. Full-Heusler alloys generally exhibit strong ferromagnetism and high Curie temperatures [1].

Half-Heusler alloys (XYZ) such as TiNiSn have the same structure as Full-Heusler alloys, except that the second sub-lattice occupied by the X atom is vacant, which results in $C1_b$ structure and $F\bar{4}3m$ symmetry [2, 4]. Half-Heusler alloys also exhibit Slater-Pauling behavior, but with a smaller number of fully occupied minority bands, usually nine (Eq. (2)). Half-Heusler alloys typically exhibit lower magnetic moments and Curie temperatures than Full-Heusler alloys [1].

$$M_t = Z_t - 18 \tag{2}$$

Inverse Heusler alloys follow the formula (X_2YZ) such as Mn_2CoAl with the second X atom moving to the third lattice and conforming to XA structure with $F\bar{4}3m$ symmetry [2]. This structure is observed when the Y element has a larger valence than the X element. These materials still exhibit Slater-Pauling behavior, but do not have a consistent number of fully occupied minority bands, which leads to a variety of potential equations, some of which are shown in Eq. (3).

* Corresponding author.
E-mail address: weverhart@kcp.com (W. Everhart).

https://doi.org/10.1016/j.heliyon.2019.e01578
Received 19 February 2019; Received in revised form 23 April 2019; Accepted 24 April 2019

$$M_t = \begin{cases} Z_t - 18 & for\ X = V, Sc, Ti \\ Z_t - 24 & for\ X = V, Cr, Mn \\ Z_t - 28 & for\ X = Cr, Mn\ and\ Y = Cu, Zn \end{cases} \quad (3)$$

Due to the inversion of the position of the second X atom in the lattice, the Y atom beings to play a role in the Slater-Pauling behavior observed. Inverse Heusler alloys are of particular interest because of the high Curie temperatures and coherent growth on semiconductors [1].

Finally, quaternary Heusler alloys (XX'YZ) such as CoFeMnSi fill all four sub-lattices with X and X', which are different transition group elements, and adhere to the same positions as the X atoms in the Full-Heusler structure and have $F\bar{4}3m$ symmetry [2]. In these systems the valence of X is higher than the valence of X' which is higher than the valance of Y. Quaternary Heusler alloys follow the same Slater-Pauling relationship as Full-Heusler alloys (Eq. (1)) [1].

Knowledge of mechanical properties of these materials has not been a significant area of research due to a focus on magnetic and electrical properties and a lack of commercialization. In their experimental work on Half-Heusler alloys for thermoelectrics, Rogl, et al [5] and He, et al [6] identify the thermal and mechanical stresses generated during thermal cycling and environmental vibrations as a key gap in understanding that must be addressed prior to commercialization. Similar considerations must be given for Heusler alloys with other applications such as ferromagnetic rotors or solenoids, spintronics, magnetic cooling, and shape memory materials, though experimental work has yet to sufficiently advance to the understanding of mechanical properties in these materials.

Due to their potential as functional magnetic shape memory alloys (MSMA), there is some work on the mechanical performance of Heusler alloys relative to martensitic transformations [7, 8, 9, 10, 11, 12, 13]. While the martensitic transformation is mechanical in nature, the transformation strain values and failure strain values are indicative of transformation induced plasticity (TRIP) which will typically yield a change in magnetic properties. Since Heusler alloys are typically of interest for their unique band structures and magnetic performance, such a change in magnetic properties is often undesirable, making the TRIP mechanical properties measured on Heusler alloys less relevant in this discussion. It should be noted that this high level of ductility may offer some pathways to larger scale manufacturing; a distinct heat treatment could be used for processing to form a martensitic phase, and another heat treatment could be used for functionalization to form the desired Heusler structure.

There are also several works that reference mechanical properties which involve non-stoichiometric Heusler alloys. These works include modeling predictions of elastic properties as the chemistry moves from one stable alloy to another [14, 15, 16], as well as doping for improvement in giant magnetocaloric effect [17], thermoelectrics [5, 6], and magnetic shape memory alloys [7, 9, 18].

This review intends to identify existing experimental and theoretical work on the mechanical properties of Heusler alloys in the context of their magnetic properties and alloy type. Magnetic properties will be discussed in the context of magnetic moment to maintain a connection to the key functional properties of these materials. While minimal experimental work has been done, conclusions are often drawn based on theoretical predictions of elastic properties. An in depth discussion of these results, as well as the validity of these methods, is included.

2. Main text

2.1. Elastic properties

The most reported elastic property for Heusler alloys is Young's modulus. The experimental methods that have been used to evaluate the Young's modulus cover a wide range of techniques such as nano-indentation (NI) and resonant ultrasound spectroscopy (RUS) [5, 6]. Rogl, et. al. [5] completed experimental work measuring the elastic properties of Half-Heusler alloys. There is a wide range of Young's modulus values (83–207 GPa), as can be seen in Fig. 1. Young's modulus experimental measurements are compared to available atomistic predictions as calculated at zero Kelvin ambient temperature and zero Pascals ambient pressure [5, 6, 19, 20] in Fig. 1. The available atomistic predictions for comparison to experimental Young's modulus are for TiNiSn [19] and ZrNiSn [20]. TiNiSn is over-predicted by 50 GPa and ZrNiSn is under predicted by 7 GPa. It is interesting to note that all experimental results were generated at room temperature, thus a matching value generated by simulations which assume zero Kelvin may not be produce a good prediction.

He, et. al. [6] also measured elastic properties of both p-type and n-type half-Heusler based thermoelectrics. The p-type material is (Hf/Zr)CoSb doped with Ti and Sn ($Hf_{0.44}Zr_{0.44}Ti_{0.12}CoSb_{0.8}Sn_{0.2}$) and the n-type material is (Hf/Zr)NiSn doped with Sb ($Hf_{0.25}Zr_{0.75}NiSn_{0.99}Sb_{0.01}$). Notably, the n-type material is based on the ZrNiSn half-Heusler alloy reported on in Rogl, et. al. [5] and the Young's modulus measurements closely match (within 2 GPa), which indicates minimal impact of doping on the stiffness of the material.

Bulk modulus of Heusler alloys were also reported by Rogl, et. al. [5] (Fig. 2). Values span a smaller range, though this is likely due to the small number of measurements. Again, the value for TiNiSn is over-predicted by 20 GPa and the value for ZrNiSn is under-predicted by 8 GPa with atomistic modeling.

The elastic properties of Heusler alloys have been heavily investigated as part of atomistic modeling studies due to the use of stiffness tensor coefficients in identifying the stability of any particular crystal structure. Specifically for cubic crystals, the only non-zero stiffness coefficients are c_{11}, c_{12}, and c_{44} and the stability requirements are shown in Eqs. (4), (5), (6), and (7) [3, 4, 7, 14, 15, 16, 18, 21, 22, 23, 24, 25, 26, 27, 28, 29, 30, 31, 32, 33, 34, 35, 36, 37, 38, 39, 40, 41, 42, 43, 44, 45, 46, 47, 48, 49].

$$c_{11} > 0 \quad (4)$$

$$c_{44} > 0 \quad (5)$$

$$c_{11} - c_{12} > 0 \quad (6)$$

$$c_{11} + 2c_{12} > 0 \quad (7)$$

The modeling of stiffness of a crystal structure is well established using density functional theory (DFT) and once stability is determined, an approximation of bulk modulus (Eq. (8)) [3, 7, 14, 18, 24, 25, 26, 29, 30, 31, 34, 35, 36, 37, 38, 39, 42, 44, 45, 47] and the Voigt-Reuss-Hill approximation of shear modulus (Eqs. (9), (10), and (11)) [3, 4, 7, 14, 18, 21, 22, 23, 24, 25, 26, 27, 28, 30, 31, 32, 35, 37, 39, 41, 42, 44, 47, 48, 49] can be applied. It is worth noting that DFT calculations are typically performed at zero Pascals and zero Kelvin.

$$B = 1/3\,(c_{11} + 2c_{12}) \quad (8)$$

$$G_V = 1/5\,(c_{11} - c_{12} + 3c_{44}) \quad (9)$$

$$G_R = 5c_{44}(c_{11} - c_{12})/4c_{44} + (c_{11} - c_{12}) \quad (10)$$

$$G = 1/2\,(G_V + G_R) \quad (11)$$

Where B is the bulk modulus, G_v is the Voigt shear modulus, G_r is the Reuss shear modulus, and G is the Voigt-Reuss-Hill approximation for shear modulus. Collected values for predictions of shear modulus can be seen in Fig. 3. Half-Heusler alloys tend to have only low magnetic moments and lower modulus values while quaternary, full and inverse materials cover the entire range of magnetic moments and tend to have higher modulus values. Young's modulus (Fig. 4) and Bulk modulus (Fig. 5) show similar trends with respect to magnetic moment, with Half-

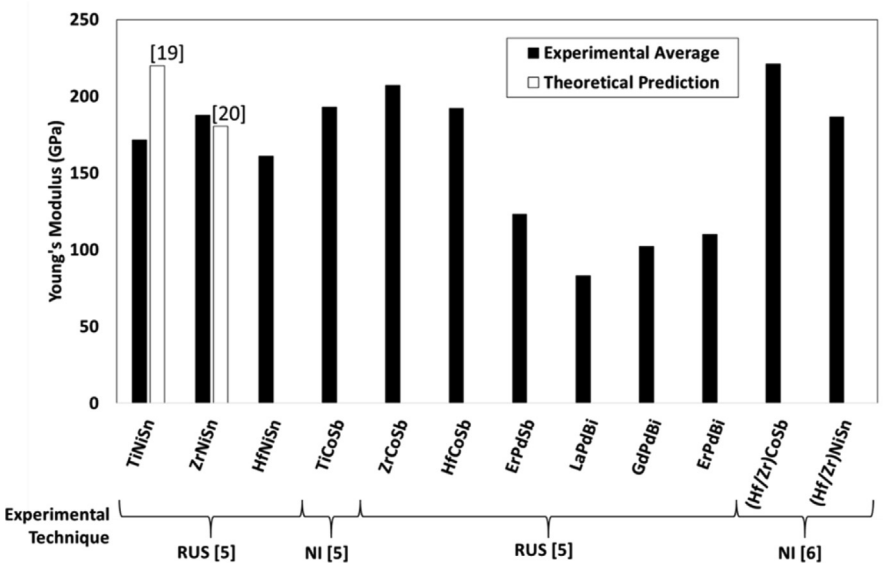

Fig. 1. Young's modulus experimental measurements compared to available atomistic predictions as calculated at zero Kelvin ambient temperature and zero Pascals ambient pressure [5, 6, 19, 20].

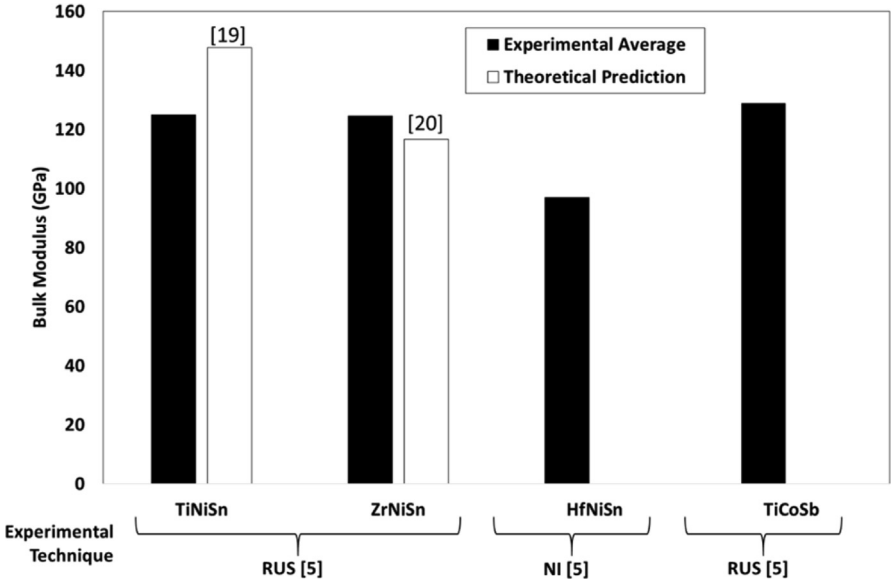

Fig. 2. Bulk modulus experimental measurements compared to available atomistic predictions as calculated at zero Kelvin ambient temperature and zero Pascals ambient pressure [5, 19, 20].

Heusler alloys having particularly low bulk modulus values, the only extremely low values occur in Half-Heusler alloys.

Several publications specifically seek to address the effects of increased pressure or temperature on the properties of Heusler alloys. Overall, these publications use DFT and predict an increase in each stiffness coefficient as pressure increases and a decrease in elastic moduli with increasing temperature. Wen, et. al. [48] demonstrates increasing stiffness tensor coefficients, and thus increasing elastic moduli for Ni_2ScAl, Ni_2TiAl, and Ni_2VAl. As can be seen for Ni_2ScAl (Fig. 6), pressure has the largest effect on c_{11}, followed by c_{12} and c_{44}. This increases elastic moduli, with bulk and Young's modulus increasing a larger amount with increased pressure than shear modulus (Fig. 7). Wen, et. al. [48] also investigated the effect of increasing temperature on the elastic moduli and reports decreasing stiffness as a function of increasing temperature over approximately 100K.

Figs. 8 and 9 compile all the available information on the effects of ambient pressure on the elastic moduli of Heusler alloys by comparing the rate of increase for each value [22, 26, 31, 48, 60, 65]. It is worthy to note that all values reported are for Full-Heusler alloys except for one Half-Heusler alloy. As was evident for Ni_2ScAl, all other materials show increasing tensor coefficients and increasing elastic properties with increasing pressure. The relative rates of increase also hold for all reported values; c_{11} increases faster than c_{12} which increases faster than c_{44}, and bulk modulus and Young's modulus increase faster than shear modulus.

Though experimental data is limited, the high numbers of reported simulation values allow for some comparisons to be made between the elastic properties of Heusler alloys and ceramics or metals (Fig. 10). Both experimental and calculated predictions for Heusler alloys lie within the field representing metals and trend towards higher modulus values.

Bulk modulus and Young's modulus values follow similar trends between Heusler alloy classes with Half-Heusler alloys having the lowest

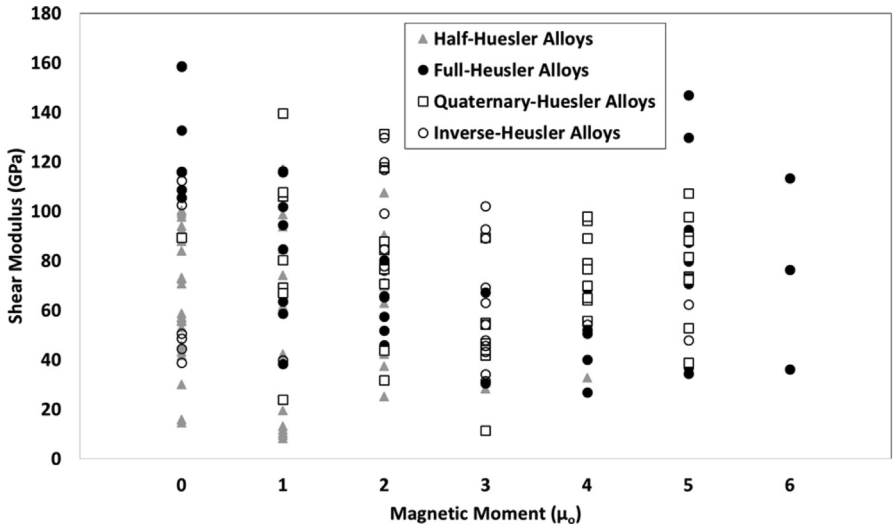

Fig. 3. Shear Modulus organized by magnetic moment (calculated from the Slater-Pauling rule) for stable Heusler alloys predicted using quantum mechanics simulations [3, 4, 7, 14, 15, 16, 21, 22, 23, 24, 25, 26, 27, 28, 29, 30, 31, 32, 33, 34, 35, 36, 37, 38, 39, 40, 41, 42, 43, 44, 45, 46, 47, 48, 49, 50, 51, 52, 53, 54, 55, 56, 57, 58, 59, 60, 61, 62, 63, 64, 65, 66, 67, 68, 69, 70, 71, 72, 73, 74, 75, 76, 77, 78, 79, 80, 81, 82, 83, 84, 85, 86, 87, 88, 89, 90, 91].

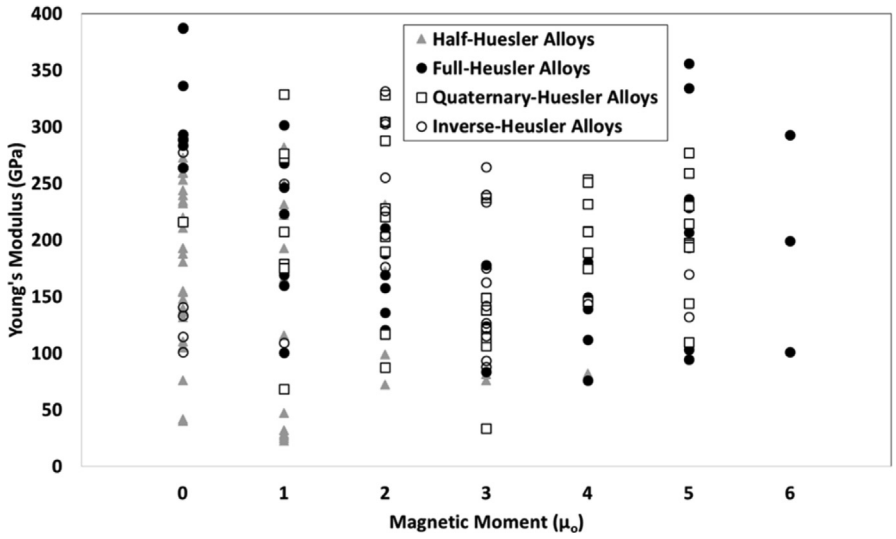

Fig. 4. Young's modulus organized by magnetic moment (calculated from the Slater-Pauling rule) for stable Heusler alloys predicted using quantum mechanics simulations [3, 4, 7, 14, 15, 16, 21, 22, 23, 24, 25, 26, 27, 28, 29, 30, 31, 32, 33, 34, 35, 36, 37, 38, 39, 40, 41, 42, 43, 44, 45, 46, 47, 48, 49, 50, 51, 52, 53, 54, 55, 56, 57, 58, 59, 60, 61, 62, 63, 64, 65, 66, 67, 68, 69, 70, 71, 72, 73, 74, 75, 76, 77, 78, 79, 80, 81, 82, 83, 84, 85, 86, 87, 88, 89, 90, 91].

values. Quaternary-Heusler, Inverse-Heusler, and Full-Heusler alloys have the highest values. Bulk modulus values for each class of Heusler alloy span a wider range, and except for some Half-Heusler alloys with extremely low values of bulk modulus, no trends appear. Additionally, analysis of the properties of Heusler alloys as a function of increasing pressure or temperature indicates that elastic properties decrease with increasing temperature above 100K and increase with increasing pressure up to 50 GPa.

2.2. Hardness & strength

Experimental scope for the hardness of Heusler alloys is extremely limited. Rogl, et. al [5], and He, et. al [6], both report values for hardness using Vicker's hardness (HV) or nano-hardness (NI) (Fig. 11). In order to allow for comparison of values from the two methods, Rogl, et. al. [5] leverages the linear conversion shown in Eq. (12).

$$H = HV * 0.0108 \tag{12}$$

In Eq. (12), H is the hardness in GPa, HV is the Vicker's hardness, and 0.0108 is the conversion factor. Rogl et. al. [5] also investigated the stability of nanohardness measurement results as a function of indent load. They observed that for loads greater than 20 mN, the variance of the results stabilizes at around 2 GPa. The DFT calculated values for TiNiSn and ZrNiSn overestimate the hardness of the material by 4.7 and 2.3 GPa respectively. This is in contrast to the predictions for elastic properties discussed above where TiNiSn was over-predicted and ZrNiSn was slightly under-predicted. This indicates that Yousef's approximation may be over-predicting hardness values. The value reported by He, et. al. [6] for hardness of the doped (Hf/Zr)NiSn (9.1 GPa) is in close agreement with the value reported by Rogl, et al. [5] for ZrNiSn (10.2 GPa) (Fig. 11).

Very little information is present discussing the strength of Heusler alloys and there is no available method for predicting the strength of these materials from the simulation data available. Musabirov, et. al. [17] performed compression testing on off-stoichiometric Ni_2MnIn at elevated temperatures. At 773 K, the material reached a peak stress of approximately 475 MPa, while at 973 K, the peak stress was reduced below 200

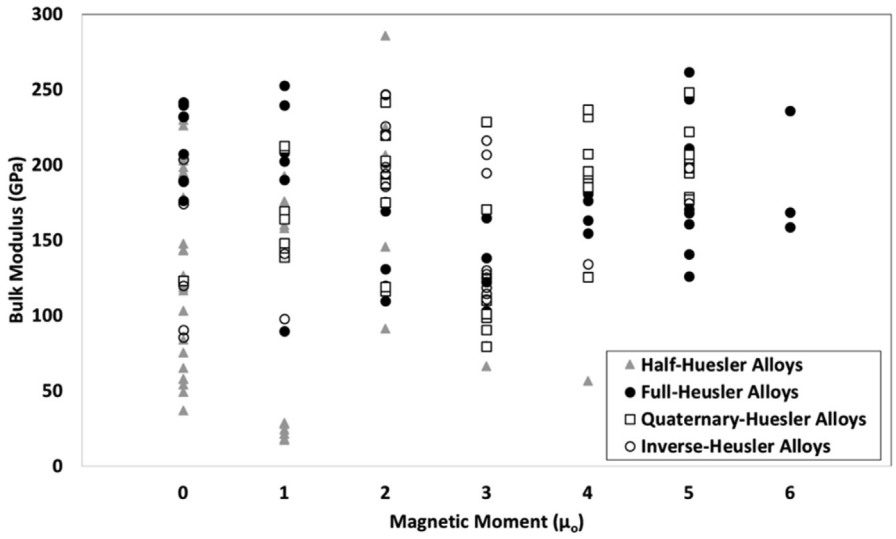

Fig. 5. Bulk modulus organized by magnetic moment (calculated from the Slater-Pauling rule) for stable Heusler alloys predicted using quantum mechanics simulations [3, 4, 7, 14, 15, 16, 21, 22, 23, 24, 25, 26, 27, 28, 29, 30, 31, 32, 33, 34, 35, 36, 37, 38, 39, 40, 41, 42, 43, 44, 45, 46, 47, 48, 49, 50, 51, 52, 53, 54, 55, 56, 57, 58, 59, 60, 61, 62, 63, 64, 65, 66, 67, 68, 69, 70, 71, 72, 73, 74, 75, 76, 77, 78, 79, 80, 81, 82, 83, 84, 85, 86, 87, 88, 89, 90, 91].

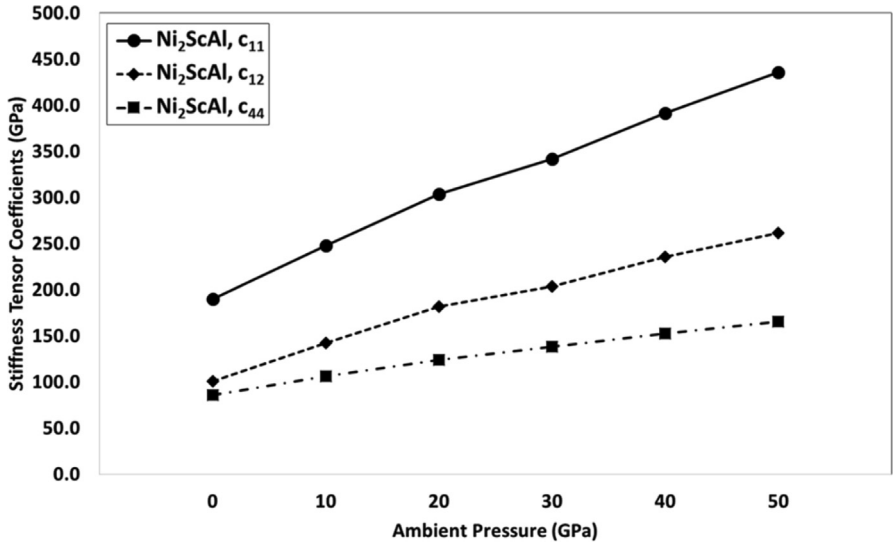

Fig. 6. Stiffness tensor coefficients as a function of ambient pressure [48].

MPa. This reduction in flow stress may provide some insight into methods for processing Heusler alloys, but further work is needed to ensure that the material does not retain significant amounts of damage after processing, which could impact magnetic performance.

Yang, et. al. [18] used an atomistic modeling method where a unidirectional strain was imposed to a single crystal. Perpendicular strain was then allowed to relax until stress was below 0.1 GPa. Finally, stress was calculated as a function of the applied strain and Young's modulus. The stress values for this analysis ranged from 0 to 11 GPa, which indicates that they may be representative of the theoretical strength of the material strength (E/10 = 19.2 GPa), but not actual yield or failure strength values. This is likely the case due to inability of the model to generate dislocations in the crystal structure. The simulation method does identify a phase transformation after reaching approximately 4 GPa through both a decrease in stress as well as a change in magnetic properties.

There are a number of examples of compression testing for evaluation of the martensitic transformations of Heusler alloys. Maziarz, et al [10] evaluated off-stoichiometric NiMnSn with indium additions manufactured as melt spun ribbons with martensitic structure. They observed that as they added indium dopant, a reduction in peak stress was observed during compression from ~2200 MPa to less than 500 MPa. It is unclear what percentage of this strength reduction was due to the observed increase in porosity with indium additions. Jiang, et al [9] also evaluated the martensitic transformation and mechanical properties in compression of several materials and identified failure stresses in excess of 2200 MPa. Hsu, et al [11] investigated the effect of aluminum additions to NiTiHf Half-Heusler alloys and observed an increase in the strength as a function of the aluminum content up to ~1500 MPa at 3% strain. Additionally, they observed a martensitic transformation during the room temperature compression test above 3% aluminum addition. Huang, et al [12] also evaluated the peak compressive strength of a fully martensitic structure at approximately 800 MPa.

Elastic property modeling with DFT can be further extended, through Yousef's approximation (Eq. (13)) [5] to provide an indication of hardness (Fig. 12).

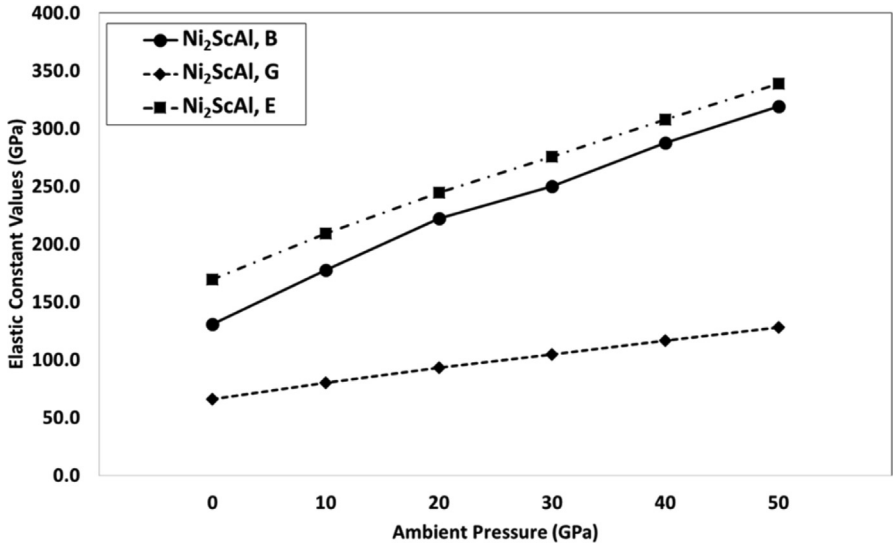

Fig. 7. Bulk and shear modulus values as a function of ambient pressure [48].

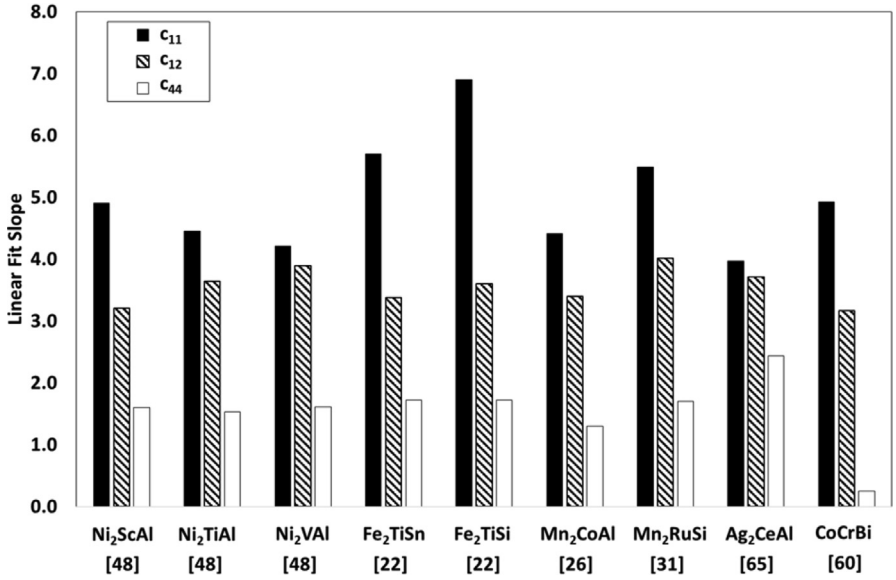

Fig. 8. Rate of increase for stiffness tensor coefficients as a function of pressure [22, 26, 31, 48, 60, 65].

$$H = \frac{(1-2\nu)E}{6(1+\nu)} \tag{13}$$

In Eq. (13), E is the Young's modulus and ν is the Poisson's ratio. No clear trends are present as a function of magnetic moment and similar to what was observed in the elastic properties, Half-Heusler alloys tend to have the lowest hardness values and Inverse-Heusler and Quaternary-Heusler alloys tend to have the highest values.

Rogl, et. al. [5], proposed a linear relationship between hardness and elastic modulus based on experimental results shown in Eqs. (14)), (15).

$$H = 0.0467E \tag{14}$$

In Eq. (14), H is the hardness in GPa and E is Young's modulus. This proposed relationship is shown in Fig. 13 compared to the collected simulation and experimental data. Overall, the fit to experimental data as well as simulation results is fairly good. Approximately 50% of the predicted hardness values, and three of six experimental values fall within the 80% confidence interval. Of the remaining values, nearly all predictions lie above the proposed fit, as well as all three remaining experimental values. The proposed model by Rogl, et al [5] provides a decent approximation of hardness given only the Young's modulus of the material, though it might be argued that Yousef's approximation may provide a better generalized agreement between simulation and experimental data by incorporating Poisson's ratio. However, when compared to experimental data seen above, Yousef's approximation appears to overestimate hardness. Not enough experimental data exists to draw a solid conclusion as to which approximation is better, or if either is valid.

Applying Yousef's approximation to the simulation results for elastic properties of Heusler alloys enables some analysis of the expected trends for hardness as a function of pressure. As might be expected by the increasing elastic properties, hardness increases as pressure increases (Fig. 14). Most results appear to follow a linear trend, but Mn_2CoAl and CoCrBi both show more polynomial trends. Mn2CoAl peaks in hardness around 20 GPa, but there is no data beyond 25 GPa. CoCrBi also peaks at 20 GPa, though data up to 50 GPa shows a continuing decrease in hardness past the peak. More data, especially experimental data, is needed to adequately understand the relationship between hardness and pressure.

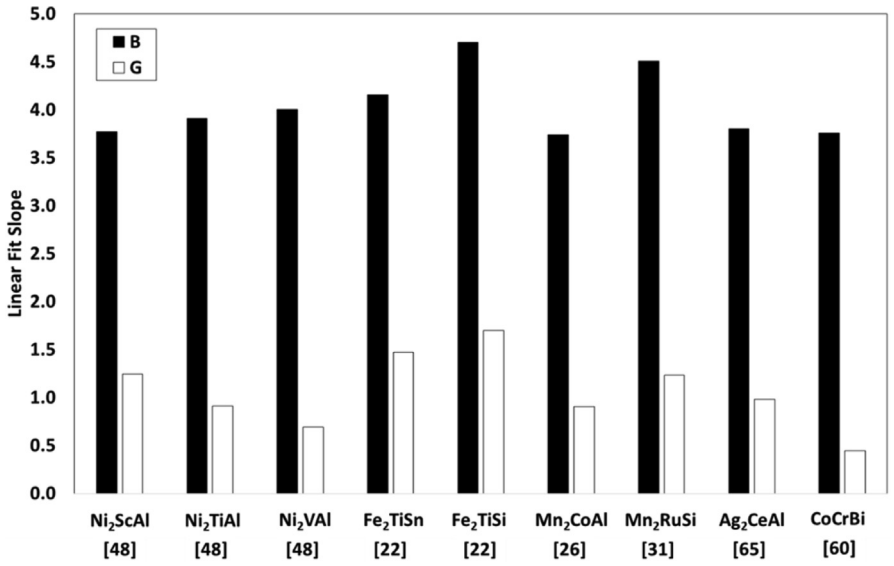

Fig. 9. Rate of increase for elastic moduli as a function of pressure [22, 26, 31, 48, 60, 65].

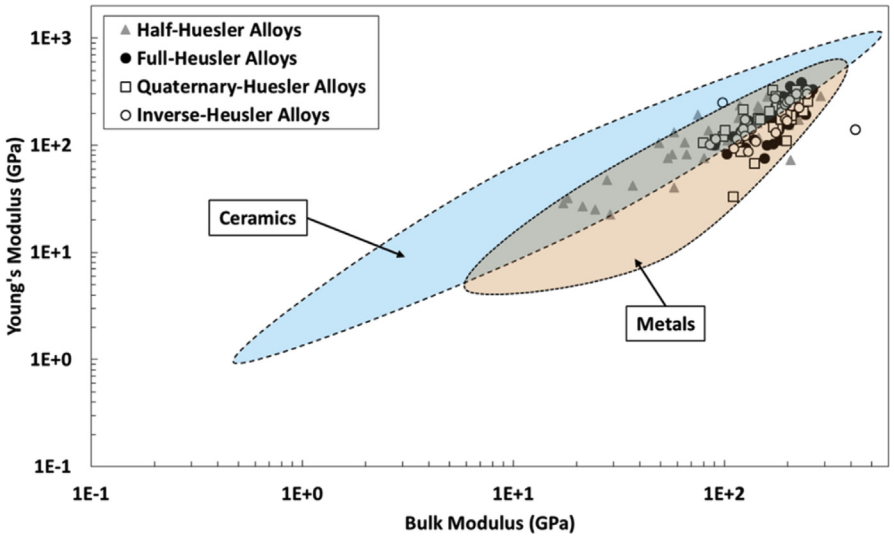

Fig. 10. Young's modulus versus bulk modulus DFT predictions for Heusler alloys as compared to metals and ceramics [3, 4, 7, 14, 15, 16, 21, 22, 23, 24, 25, 26, 27, 28, 29, 30, 31, 32, 33, 34, 35, 36, 37, 38, 39, 40, 41, 42, 43, 44, 45, 46, 47, 48, 49, 50, 51, 52, 53, 54, 55, 56, 57, 58, 59, 60, 61, 62, 63, 64, 65, 66, 67, 68, 69, 70, 71, 72, 73, 74, 75, 76, 77, 78, 79, 80, 81, 82, 83, 84, 85, 86, 87, 88, 89, 90, 91]. Metal and Ceramic regions determined from the Material Universe dataset from GRANTA MI, Granta Design Limited, Cambridge, UK, 2019.

There are significant gaps in knowledge of the hardness and strength of Heusler alloys. While the hardness of some of these materials has been measured, experimental values are limited to only a few Half-Heusler alloys. Atomistic modeling results appear to be sufficient to give an indication of hardness value trends, though they assume that Yousef's approximation is applicable to all Heusler alloy classes. As can be seen in Fig. 15, the predicted hardness of Heusler alloys range from 1 GPa, in the middle of hardness values for metals, to over 30 GPa, well into the range of hardness values for ceramics. Half-Heusler alloys also appear to have higher hardness with lower Young's modulus values. It is not clear from the available data, but it appears possible that the potential over-prediction of hardness by Yousef's approximation may be exclusive to Half-Heusler alloys, though there is no hardness data for any other Heusler alloy class. DFT results also indicate, as expected, that as pressure is increased, hardness increases, but a precise knowledge of this trend and its limit has not yet been determined.

There is not enough information to make a good judgement regarding the range of expected room temperature strength for Heusler alloys, but based on elevated temperature tests exhibiting peak values up to 475 MPa, room temperature strength can be expected to be higher. This indicates that values are likely to remain within the range occupied by engineering metals and ceramics. Experimental and simulation work on martensitic transformations indicate that high peak stress values can be achieved, but it is unclear if these values are solely due to the martensitic transformation or if magnetic properties can be maintained up to these stress values.

2.3. Fracture toughness, malleability & ductility

The preference of a material to deform rather than fracture can be evaluated in several ways such as fracture toughness, ductility, or malleability. The fracture toughness of a material is specifically the threshold required for a crack of specific size within a material to propagate. The only measurements of fracture toughness in Heusler alloys were performed by Rogl, et. al [5] leveraging a method for approximating fracture toughness from Vickers hardness results (Eqs. (14), (15).

$$K_C = \beta\left(\frac{E}{HV}\right)^{1/2}\frac{F}{c^{3/2}} \tag{15}$$

In Eq. (15), E is Young's modulus, HV is Vickers hardness, F is the indentation load (1 N [5]), c is the radial crack length from the center of

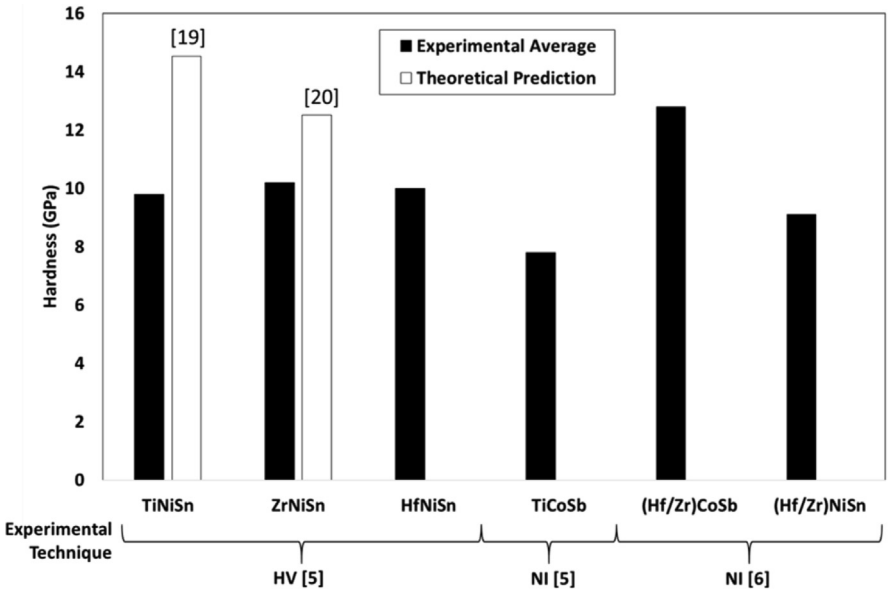

Fig. 11. Hardness experimental measurements compared to available atomistic predictions as calculated at zero Kelvin ambient temperature and zero Pascals ambient pressure [5, 6, 19, 20].

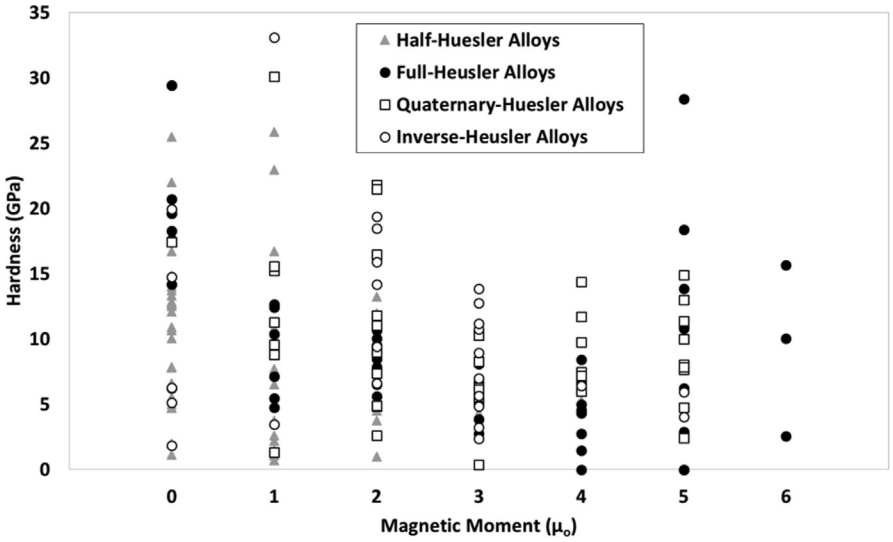

Fig. 12. Hardness values predicted by Yousef's approximation organized by magnetic moment (calculated from the Slater-Pauling rule) for stable Heusler alloys predicted using quantum mechanics simulations [3, 4, 7, 14, 15, 16, 21, 22, 23, 24, 25, 26, 27, 28, 29, 30, 31, 32, 33, 34, 35, 36, 37, 38, 39, 40, 41, 42, 43, 44, 45, 46, 47, 48, 49, 50, 51, 52, 53, 54, 55, 56, 57, 58, 59, 60, 61, 62, 63, 64, 65, 66, 67, 68, 69, 70, 71, 72, 73, 74, 75, 76, 77, 78, 79, 80, 81, 82, 83, 84, 85, 86, 87, 88, 89, 90, 91].

the indentation, and β is a function of the indenter angle (0.016 [5]). Values were measured by Rogl, et al. [5] between 1.3 and 2.3 MPa $m^{1/2}$, indicating low fracture toughness of Heusler alloys. Shear modulus, and thus Pugh's criteria [93] (Eq. (15)), can also be calculated from the experimental data provided by Rogl, et al [5].

$$P = {}^{B}/_{G} \tag{16}$$

In Eq. (16), G is the shear modulus and B is the bulk modulus. This allows for a comparison of the fracture toughness values reported above with the predicted malleability. In the case of TiNiSn, fracture toughness values are reported as 1.86, a relatively low number, and Pugh's criteria is 1.85, a number sufficient for malleability. ZrNiSn has a higher fracture toughness of 2.1, but a lower Pugh's ratio of 1.65, with both values indicating brittle behavior. And finally, HfNiSn has a fracture toughness of 2.17, the highest value calculated, but has the lowest Pugh's ratio with a value of 1.47. These discrepancies between low values for fracture toughness and Pugh's ratio values that indicate malleability highlight a potentially major flaw in the use of Pugh's ratio when applied to crack formation and fracture in intermetallics.

Some testing of strain to failure in compression has been completed, though most of it is in the context of martensitic transformations in MSMAs. Compression testing by Musabirov, et. al. [17] exhibited deformation of up to approximately 1.5 true strain at 773 K, with significant pores and cracking present in the deformed structure. At 873 K, the material only exhibits a small amount of cracking, but shows significant amounts of dynamic recrystallization of up to 1.8 true strain. These values give an indication of malleability at elevated temperature and room temperature properties can be expected to be significantly lower. Maziarz, et al [10] observed strain to failure in compression from 1% to 5% for martensitic material. They observed a significant reduction in strain to failure with increasing amounts of indium, but the cause of this was attributed to increased porosity. Jiang, et al [9] identified strains to failure of 17–20% in martensitic material, though they suggest that the high values should only be treated as qualitative values due to machine compliance. Huang, et al [12] evaluated strains to failure of material exhibiting martensitic transformations of up to 5%.

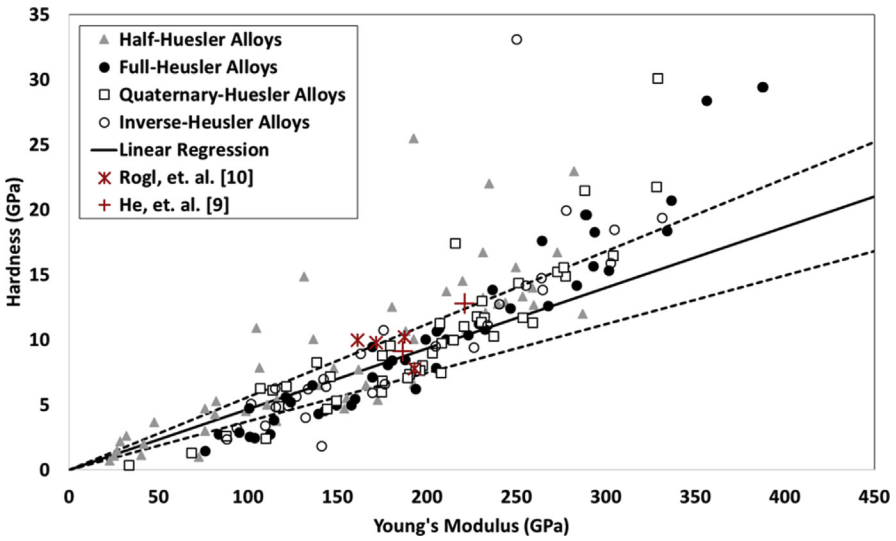

Fig. 13. Hardness values predicted by Yousef's approximation as a function of Young's modulus for stable Heusler alloys predicted using quantum mechanics simulations 3, 4, 5, 6, 7, 14, 15, 16, 21, 22, 23, 24, 25, 26, 27, 28, 29, 30, 31, 32, 33, 34, 35, 36, 37, 38, 39, 40, 41, 42, 43, 44, 45, 46, 47, 48, 49, 50, 51, 52, 53, 54, 55, 56, 57, 58, 59, 60, 61, 62, 63, 64, 65, 66, 67, 68, 69, 70, 71, 72, 73, 74, 75, 76, 77, 78, 79, 80, 81, 82, 83, 84, 85, 86, 87, 88, 89, 90, 91]. Experimental results from Rogl, et. al. [5] are included along with the predicted linear relationship and an 80% confidence interval.

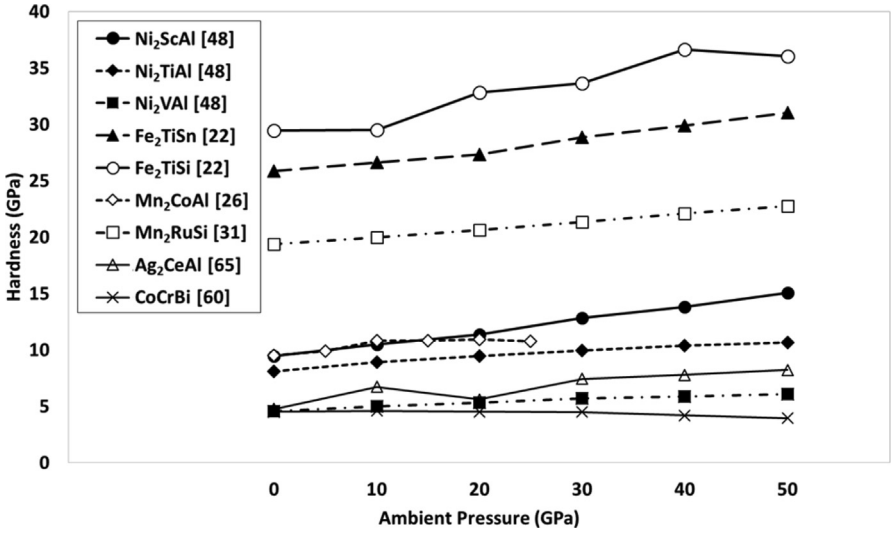

Fig. 14. Hardness (predicted through Yousef's approximation) as a function of ambient pressure [22, 26, 31, 48, 60, 65].

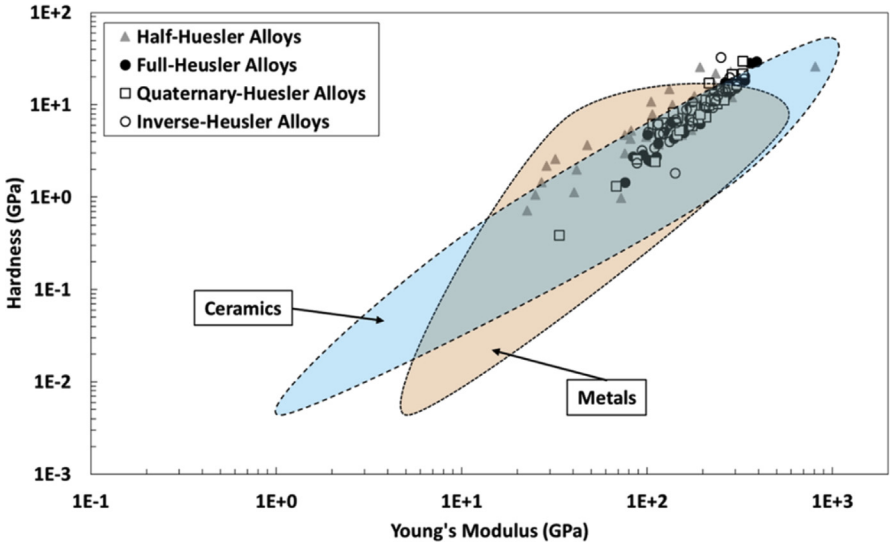

Fig. 15. Elastic modulus versus hardness for Heusler alloys as compared to metals and ceramics [3, 4, 7, 14, 15, 16, 21, 22, 23, 24, 25, 26, 27, 28, 29, 30, 31, 32, 33, 34, 35, 36, 37, 38, 39, 40, 41, 42, 43, 44, 45, 46, 47, 48, 49, 50, 51, 52, 53, 54, 55, 56, 57, 58, 59, 60, 61, 62, 63, 64, 65, 66, 67, 68, 69, 70, 71, 72, 73, 74, 75, 76, 77, 78, 79, 80, 81, 82, 83, 84, 85, 86, 87, 88, 89, 90, 91]. Metal and Ceramic regions determined from the Material Universe dataset from GRANTA MI, Granta Design Limited, Cambridge, UK, 2019.

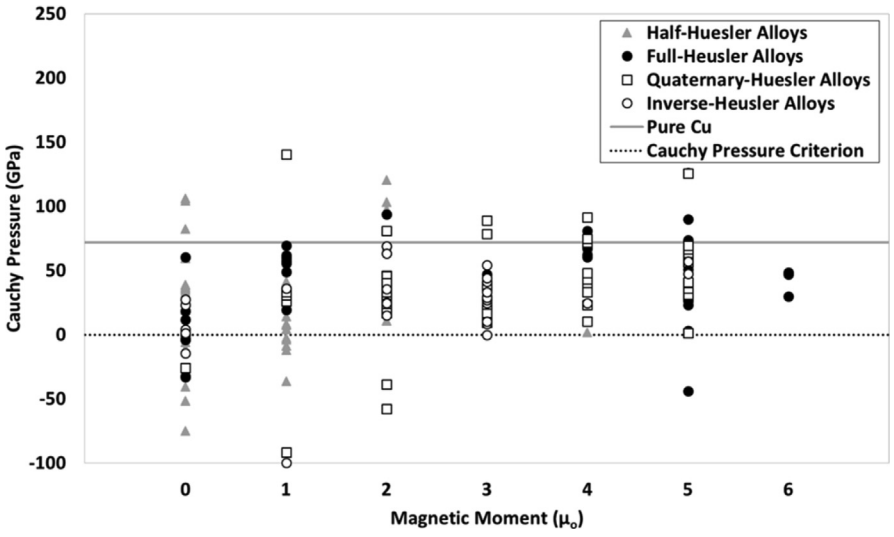

Fig. 16. Cauchy pressure values organized by magnetic moment (calculated from the Slater-Pauling rule) for stable Heusler alloys predicted using quantum mechanics simulations [3, 4, 7, 14, 15, 16, 21, 22, 23, 24, 25, 26, 27, 28, 29, 30, 31, 32, 33, 34, 35, 36, 37, 38, 39, 40, 41, 42, 43, 44, 45, 46, 47, 48, 49, 50, 51, 52, 53, 54, 55, 56, 57, 58, 59, 60, 61, 62, 63, 64, 65, 66, 67, 68, 69, 70, 71, 72, 73, 74, 75, 76, 77, 78, 79, 80, 81, 82, 83, 84, 85, 86, 87, 88, 89, 90, 91]. Cauchy pressure for Cu is presented as a reference point for ductile behavior [7].

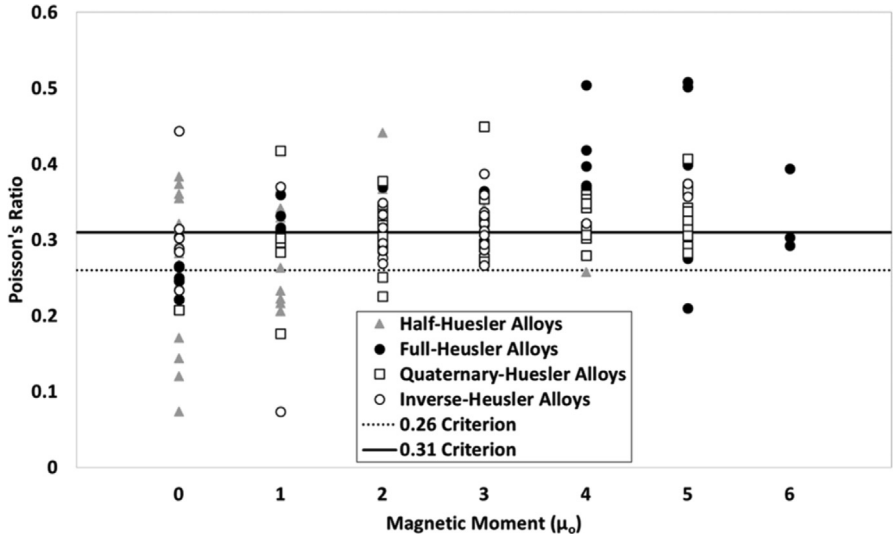

Fig. 17. Poisson's ratio values organized by magnetic moment (calculated from the Slater-Pauling rule) for stable Heusler alloys predicted using quantum mechanics simulations [3, 4, 7, 14, 15, 16, 21, 22, 23, 24, 25, 26, 27, 28, 29, 30, 31, 32, 33, 34, 35, 36, 37, 38, 39, 40, 41, 42, 43, 44, 45, 46, 47, 48, 49, 50, 51, 52, 53, 54, 55, 56, 57, 58, 59, 60, 61, 62, 63, 64, 65, 66, 67, 68, 69, 70, 71, 72, 73, 74, 75, 76, 77, 78, 79, 80, 81, 82, 83, 84, 85, 86, 87, 88, 89, 90, 91].

The only direct modeling of fracture toughness, ductility, or malleability was performed by Yang, et. al. [18] through atomistic modeling of a single crystal tensile test. This analysis is applied to Ni_2MnAl up to 2Å of deformation, which, on a 5.7888Å lattice, amounts to nearly 35% engineering strain. This model neglected any formation of dislocations or any indicator of damage or fracture, and therefore is not valuable for the evaluation of damage resistance, but it does provide insight into strain based phase transformations.

There are a variety of other methods which attempt to leverage elastic properties of materials to make a prediction about the ductility of a material. This first method is referred to as Cauchy pressure (Eq. (17)) [3, 4, 7, 23, 25, 27, 29, 30, 44, 47].

$$C_p = c_{12} - c_{44} \tag{17}$$

In Eq. (17), C_p is the Cauchy pressure and c_{12} and c_{44} are the appropriate stiffness tensor coefficients. The critical value for determining ductile versus brittle behavior is zero, with positive values exhibiting ductile behavior. Fig. 16 shows the Cauchy pressure calculated from available simulation results. No major trends appear as a function of Heusler type, though only 25 of 173 alloys are expected to exhibit brittle behavior and a majority of those are found at lower magnetic moments. Several alloys have values higher than those for pure copper, which, if a correct prediction, would indicate significant ductility.

Another metric which is proposed to provide an indication of ductile versus brittle behavior is Poisson's ratio. By leveraging the simulation predictions for bulk modulus and shear modulus, Poisson's ratio can be calculated (Eq. (18)).

$$\nu = \frac{2B - 2G}{2(3B + G)} \tag{18}$$

In Eq. (18), B is the bulk modulus and G is the shear modulus. There are two commonly reported thresholds for ductile behavior: values exceeding 0.26 [23, 24, 41, 44, 47, 92] and values exceeding 0.33 [3, 7, 31, 39, 42]. Using 0.26 as the criteria yields 146 materials with ductile behavior, nearly the same number as observed with Cauchy pressure (Fig. 17). It is also apparent that the majority of low Poisson's ratio values are found at low magnetic moment. When using 0.33, that number reduces to 87.

The final and most common method for predicting ductile versus brittle behavior from elastic properties is Pugh's criteria (Eq. (16)) [93].

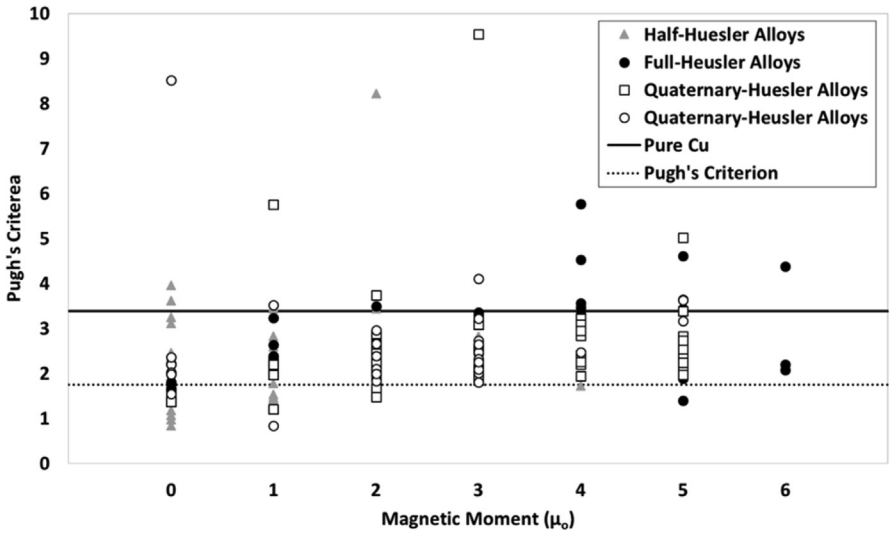

Fig. 18. Pugh's criteria values organized by magnetic moment (calculated from the Slater-Pauling rule) for stable Heusler alloys predicted using quantum mechanics simulations [3, 4, 7, 14, 15, 16, 21, 22, 23, 24, 25, 26, 27, 28, 29, 30, 31, 32, 33, 34, 35, 36, 37, 38, 39, 40, 41, 42, 43, 44, 45, 46, 47, 48, 49, 50, 51, 52, 53, 54, 55, 56, 57, 58, 59, 60, 61, 62, 63, 64, 65, 66, 67, 68, 69, 70, 71, 72, 73, 74, 75, 76, 77, 78, 79, 80, 81, 82, 83, 84, 85, 86, 87, 88, 89, 90, 91]. Pugh's criteria for pure Cu is presented as a reference point for ductile behavior [7].

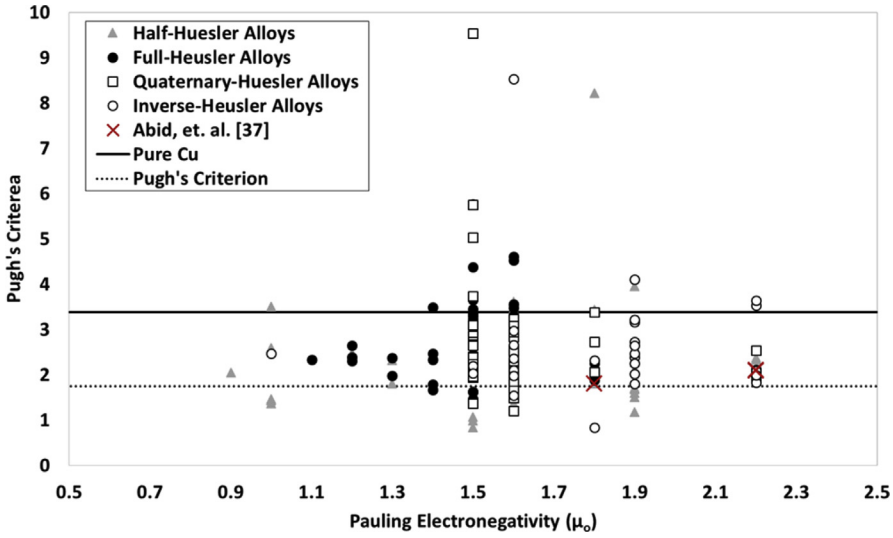

Fig. 19. Pugh's criteria values versus electronegativity (per the Pauling scale [94]) for stable Heusler alloys predicted using quantum mechanics simulations [3, 4, 7, 14, 15, 16, 21, 22, 23, 24, 25, 26, 27, 28, 29, 30, 31, 32, 33, 34, 35, 36, 37, 38, 39, 40, 41, 42, 43, 44, 45, 46, 47, 48, 49, 50, 51, 52, 53, 54, 55, 56, 57, 58, 59, 60, 61, 62, 63, 64, 65, 66, 67, 68, 69, 70, 71, 72, 73, 74, 75, 76, 77, 78, 79, 80, 81, 82, 83, 84, 85, 86, 87, 88, 89, 90, 91]. Pugh's criteria for Cu is presented as a reference point for ductile behavior [7].

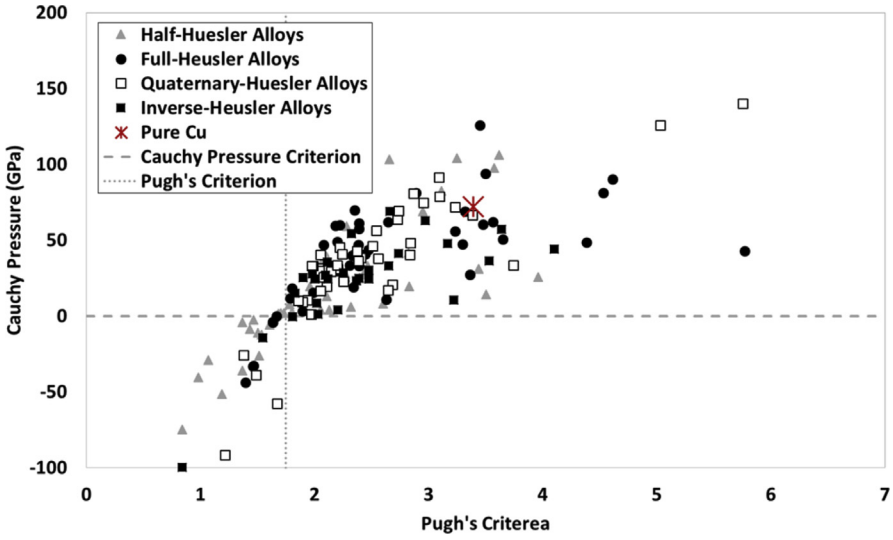

Fig. 20. Cauchy pressure values versus Pugh's criteria values for stable Heusler alloys predicted using quantum mechanics simulations [3, 4, 7, 14, 15, 16, 21, 22, 23, 24, 25, 26, 27, 28, 29, 30, 31, 32, 33, 34, 35, 36, 37, 38, 39, 40, 41, 42, 43, 44, 45, 46, 47, 48, 49, 50, 51, 52, 53, 54, 55, 56, 57, 58, 59, 60, 61, 62, 63, 64, 65, 66, 67, 68, 69, 70, 71, 72, 73, 74, 75, 76, 77, 78, 79, 80, 81, 82, 83, 84, 85, 86, 87, 88, 89, 90, 91]. Cauchy pressure and Pugh's criteria for Cu is presented as a reference point for ductile behavior [7].

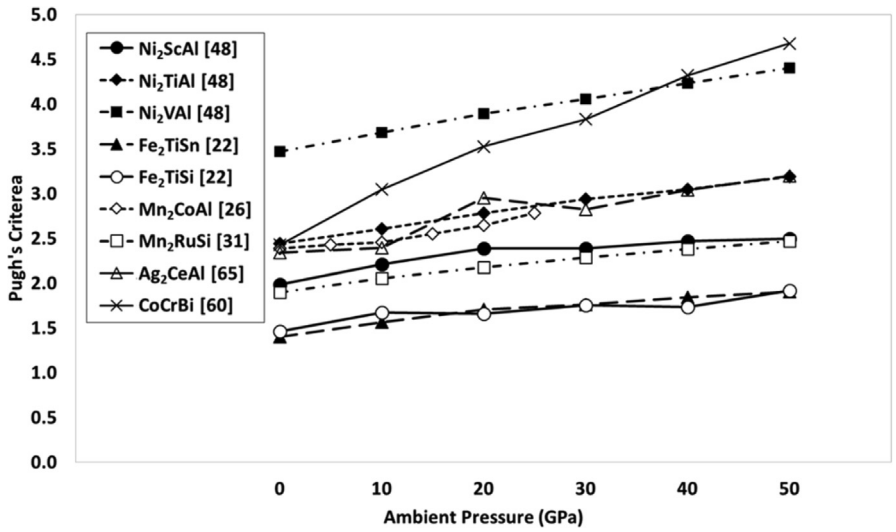

Fig. 21. Pugh's Criteria as a function of ambient pressure [22, 26, 31, 48, 60, 65].

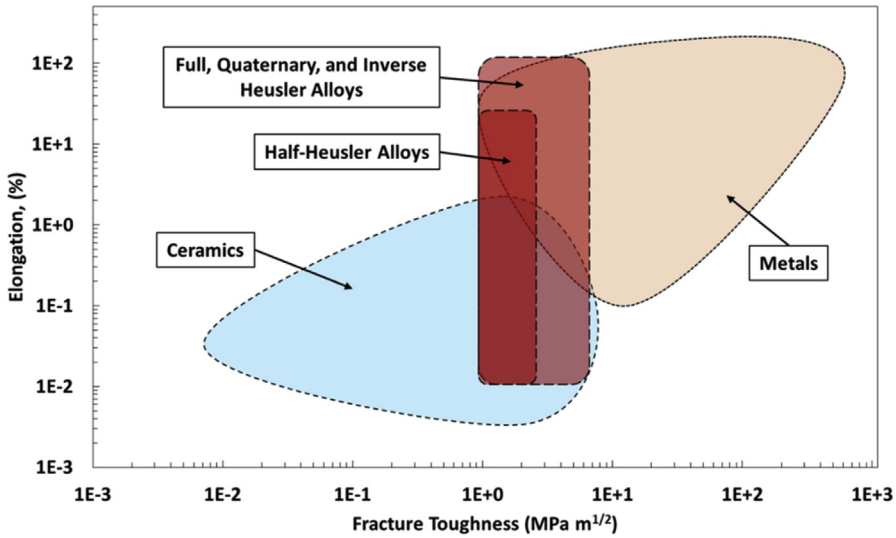

Fig. 22. Fracture toughness versus ductility for Heusler alloys as compared to metals and ceramics. Since no elongation information exists for Heusler alloys, Pugh's criteria is used as an indicator. Metal and Ceramic regions determined from the Material Universe dataset from GRANTA MI, Granta Design Limited, Cambridge, UK, 2019.

It is important to note that Pugh [93] specifically identifies that this relationship is not indented to predict ductility, but rather malleability. The common criteria above which ductile behavior is predicted is 1.75 [3, 14, 15, 16, 18, 21, 22, 23, 24, 25, 26, 27, 28, 29, 30, 32, 35, 37, 39, 42, 44, 47, 49]. Fig. 18 shows calculated values for Pugh's criteria from DFT simulations organized by magnetic moment. It can be seen that 143 of the materials are predicted to have ductile behavior and 25 are predicted to be more malleable than pure copper.

Abid, et. al. [37] proposed a relationship between Pugh's ratio and electronegativity of the second or Y atom. Fig. 19 shows the proposed relationship among the collected data for Pugh's criteria. It can be seen for the data collected by Abid, et. al. [37] for Half-Heusler alloys NbFeSb, NbRuSb, and NbOsSb that a trend may be present, but the remaining data does not support the existence of a trend.

Maziarz, et. al. [10], and Roy, et. al. [7] both discuss a proportional relationship between Cauchy pressure and Pugh's criteria. It can be seen in Fig. 20 that some relationship does exist, though a specific relationship has not been identified. The Cauchy pressure appears to reach a limit around 100 GPa while Pugh's criteria continues to increase, creating a deviation from linearity. There is also a clear inflection point in the data near the convergence of the two criteria indicating that both are indeed representing the same phenomenon.

Similar to elastic properties and hardness discussed above, Pugh's criteria increases as ambient pressure increases (Fig. 21). This effect is observed because of the higher rate of increase for bulk modulus compared to shear modulus, which is in turn driven by the more significant impact of pressure on c_{11} and c_{12} than c_{44}. It can also be seen that materials with a higher Pugh criteria at zero Pascals tend to increase at a slightly rate with increasing pressure with the exception of the one Half-Heusler alloy which increases at a significantly higher rate.

There is essentially no available experimental data for the ductility of Heusler alloys, and extremely little information on fracture toughness or malleability. The small amount of experimental results that are present indicate that Heusler alloys are brittle even up to elevated temperatures. There are also several methods that have been devised to predict ductile versus brittle behavior from elastic properties, the most common of which is Pugh's criteria, which is originally intended to approximate malleability. It is important to note that Pugh's criteria is a comparison of a single crystal's ease of plastic shear versus fracture [93] and that the criteria is a proportionality which applies within a single crystal structure

for a single burger's vector. In other words, the ratio of lattice parameter to burger's vector is constant. This approach can only be effective in comparing Heusler alloys if the same assumptions can be used, which appears to be the case for at least those purely stoichiometric Heusler alloys of identical structure or type.

One of the main assumptions in existing DFT predictions for ductility is the lack of any crystal plasticity or incorporation of dislocations, though some experimental work to characterize dislocations in these materials has been completed. Strutt, et. al. [95] observed the preferred burger's vector for creep in Ni_2AlTi Heusler alloys is $a_0<110>$, which was contrary to the $a_0<100>$ dislocations coupled with anti-phase boundaries (APB) that have been observed in Ni2AlTi containing NiAl materials. It is proposed that the preference of $a_0<110>$ slip in Heusler alloys, compared to NiAl, which prefers $a_0<100>$ in creep, is due to the necessary dissociation of $a_0<100>$ dislocations and formation of APB's in the Heusler alloy. Since the energy of the APB is likely a significant driving force for preference of a given slip system in Heusler alloys and is not accounted for in Pugh's criteria, such comparisons between Heusler sub-classes, or even individual alloys, may only be minimally effective. As can be seen in Fig. 22, the fracture toughness of Heusler alloys tends to fall below that of metals and on the high end of ceramics. The estimate for ductility in Fig. 22 is based on Pugh's criteria, with the 1.75 threshold being centered on 0.01 elongation on the y-axis. The minimum Pugh's criteria value for Heusler alloys is assumed to extend to 0.001 and the maximum value is assumed to extend to 0.1. Based on this assumption for ductility, Heusler alloys are in the range of more ductile ceramics and less ductile metals.

3. Conclusions

Heusler alloys consist of a series of materials with a wide range of magnetic and electrical properties and have garnered a significant amount of interest in recent years. One remaining barrier to commercialization of these materials is a lack of understanding of their mechanical properties, which limits the available manufacturing methods as well as the ability to survive potential operating environments. There is some available data for the hardness and elastic moduli of Half-Heusler alloys, but similar data does not exist for other classes of Heusler alloys and the data that is available does not provide a clear enough picture of mechanical performance to enable effective design of a product. Other properties such as strength, fracture toughness, or ductility have not been explored experimentally. A robust understanding of these properties in both manufacturing environments as well as operating environments is needed to ensure predictable yield and service life of Heusler alloys.

While a lack of experimental data exists, a multitude of studies have attempted to draw conclusions about mechanical properties through DFT simulations. Without experimental validation, many of these studies are proposing fundamental relationships which may not drive valid conclusions. For example, Y element electronegativity is proposed to correlate to ductility and elastic constants are proposed to govern ductile versus brittle behavior. Development of mechanical property data is critical to correctly bounding the application of atomistic modeling results and preventing the potential for widespread use of potentially misleading conclusions.

Knowledge of several properties would provide significant benefit to the commercialization of Heusler alloys. Fracture toughness values would provide the ability to gauge cycles to failure for alloys with properties such as magnetic shape memory, giant magnetocaloric effect, and thermoelectric behavior while also giving insight into the single cycle behavior for a variety of other applications. Similarly, stress-strain relationships in both compression and tension can be of value for determining critical loading limits and factors of safety or flow stress for manufacturing purposes and can form the basis for a wide variety of temperature or strain rate effects. These and other potential properties of value should be investigated within the context of the magnetic properties of interest to ensure that the operational function of any device is not compromised by unexpected mechanical loading or damage. As the properties of these materials are more clearly understood, new areas of research into methods of optimizing Heusler alloys will likely become important.

Declarations

Author contribution statement

All authors listed have significantly contributed to the development and the writing of this article.

Funding statement

This presentation has been authored by Honeywell Federal Manufacturing & Technologies under Contract No. DE-NA0002839 with the U.S. Department of Energy.

Competing interest statement

The authors declare no conflict of interest.

Additional information

No additional information is available for this paper.

Acknowledgements

All data prepared, analyzed and presented has been developed in a specific context of work and was prepared for internal evaluation and use pursuant to that work authorized under the referenced contract. Reference herein to any specific commercial product, process or service by trade name, trademark, manufacturer, or otherwise, does not necessarily constitute or imply its endorsement, recommendation, or favoring by the United States Government, any agency thereof or Honeywell Federal Manufacturing & Technologies, LLC.

References

[1] C. Felser, A. Hirohata (Eds.), Heusler Alloys: Properties, Growth, Applications, Springer, Cham, 2016.
[2] V. Alijani, J. Winterlik, G.H. Fecher, S.S. Naghavi, C. Felser, Quaternary half-metallic Heusler ferromagnets for spintronics applications, Phys. Rev. B Condens. Matter 83 (2011) 1–7.
[3] A. Abada, K. Amara, S. Hiadsi, B. Amrani, First principles study of a new half-metallic ferrimagnets Mn2-based full Heusler compounds: Mn2ZrSi and Mn2ZrGe, J. Magn. Magn. Mater. 388 (2015) 59–67.
[4] T. Roy, A. Chakrabarti, Ab initio studies on electronic and magnetic properties of X2PtGa (X=Cr, Mn, Fe, Co) Heusler alloys, J. Magn. Magn. Mater. 423 (2017) 395–404.
[5] G. Rogl, A. Grytsiv, M. Gürth, A. Tavassoli, C. Ebner, A. Wünschek, S. Puchegger, V. Soprunyuk, W. Schranz, E. Bauer, H. Müller, M. Zehetbauer, P. Rogl, Mechanical properties of half-Heusler alloys, Acta Mater. 107 (2016) 178–195.
[6] R. He, S. Gahlawat, C. Guo, S. Chen, T. Dahal, H. Zhang, W. Liu, Q. Zhang, E. Chere, K. White, Z. Ren, Studies on mechanical properties of thermoelectric materials by nanoindentation, Phys. Status Solidi 212 (2015) 2191–2195.
[7] T. Roy, M.E. Gruner, P. Entel, A. Chakrabarti, Effect of substitution on elastic stability, electronic structure and magnetic property of Ni-Mn based Heusler alloys: an ab initio comparison, J. Alloy. Comp. 632 (2015) 822–829.
[8] K.G. Prashanth, H. Shakur Shahabi, H. Attar, V.C. Srivastava, N. Ellendt, V. Uhlenwinkel, J. Eckert, S. Scudino, Production of high strength Al85Nd8Ni5Co2 alloy by selective laser melting, Addit. Manuf. 6 (2015) 1–5.
[9] H. Jiang, X. Xu, T. Omori, M. Nagasako, J. Ruan, S. Yang, C. Wang, X. Liu, R. Kainuma, Martensitic transformation and shape memory effect at high temperatures in off-stoichiometric Co2VSi Heusler alloys, Mater. Sci. Eng. 676 (2016) 191–196.
[10] W. Maziarz, A. Wójcik, J. Grzegorek, A. Żywczak, P. Czaja, M.J. Szczerba, J. Dutkiewicz, E. Cesari, Microstructure, magneto-structural transformations and mechanical properties of Ni50Mn37.5Sn12.5-xInx (x=0, 2, 4, 6 % at.) metamagnetic shape memory alloys sintered by vacuum hot pressing, J. Alloy. Comp. 715 (2017) 445–453.
[11] D.H.D. Hsu, B.C. Hornbuckle, B. Valderrama, F. Barrie, H.B. Henderson, G.B. Thompson, M.V. Manuel, The effect of aluminum additions on the thermal,

microstructural, and mechanical behavior of NiTiHf shape memory alloys, J. Alloy. Comp. 638 (2015) 67–76.
[12] L. Huang, D.Y. Cong, L. Ma, Z.H. Nie, M.G. Wang, Z.L. Wang, H.L. Suo, Y. Ren, Y.D. Wang, Large magnetic entropy change and magnetoresistance in a Ni41Co9Mn40Sn10 magnetic shape memory alloy, J. Alloy. Comp. 647 (2015) 1081–1085.
[13] G.H. Yu, Y.L. Xu, Z.H. Liu, H.M. Qiu, Z.Y. Zhu, X.P. Huang, L.Q. Pan, Recent progress in Heusler-type magnetic shape memory alloys, Rare Met. 34 (2015) 527–539.
[14] L. Wang, X. Zhu, First-principles investigations of electronic, magnetic and thermodynamic properties of Heusler alloy Co2Mn1-xTixSn, J. Alloy. Comp. 679 (2016) 74–79.
[15] H. Abbassa, S. Hadjri-Mebarki, B. Amrani, T. Belaroussi, K. Driss Khodja, P. Aubert, Theoretical investigation of new Heusler alloys Ru2VGa1-xAlx, J. Alloy. Comp. 637 (2015) 557–563.
[16] I. Asfour, H. Rached, S. Benalia, D. Rached, Investigation of electronic structure, magnetic properties and thermal properties of the new half-metallic ferromagnetic full-Heusler alloys Cr 2 GdSi 1Àx Ge x : an ab-initio study, J. Alloy. Comp. 676 (2016) 440–451.
[17] I.I. Musabirov, I.M. Safarov, M.I. Nagimov, I.Z. Sharipov, V.V. Koledov, A.V. Mashirov, A.I. Rudskoi, R.R. Mulyukov, Fine-grained structure and properties of a Ni2MnIn alloy after a settling plastic deformation, Phys. Solid State 58 (2016) 1605–1610.
[18] S. Yang, Y. Kong, Y. Du, L. Shen, Y. Shen, First-principles prediction of structural, mechanical and magnetic properties in Ni2MnAl, Comput. Mater. Sci. 123 (2016) 52–58.
[19] G. Fiedler, P. Kratzer, Ternary semiconductors NiZrSn and CoZrBi with half-Heusler structure: a first-principles study, Phys. Rev. B 94 (2016) 1–11.
[20] M. Hichour, D. Rached, R. Khenata, M. Rabah, M. Merabet, A.H. Reshak, S. Bin Omran, R. Ahmed, Theoretical investigations of NiTiSn and CoVSn compounds, J. Phys. Chem. Solids 73 (2012) 975–981.
[21] K. Benkaddour, A. Chahed, A. Amar, H. Rozale, A. Lakdja, O. Benhelal, A. Sayede, First-principles study of structural, elastic, thermodynamic, electronic and magnetic properties for the quaternary Heusler alloys CoRuFeZ (Z = Si, Ge, Sn), J. Alloy. Comp. 687 (2016) 211–220.
[22] Z. Wen, Y. Zhao, H. Hou, B. Wang, P. Han, The mechanical and thermodynamic properties of Heusler compounds Ni2XAl (X=Sc, Ti, V) under pressure and temperature: a first-principles study, Mater. Des. 114 (2017) 398–403.
[23] K. Kaur, D.P. Rai, R.K. Thapa, S. Srivastava, Structural, electronic, mechanical, and thermoelectric properties of a novel half Heusler compound HfPtPb, J. Appl. Phys. 122 (2017).
[24] J.Y. Jong, J. Zhu, M.G. Jon, Y. Zhou, J.G. Kim, J. Yan, Theoretical investigation of stabilities and physical properties of low cost Fe-based full-Heusler materials, J. Alloy. Comp. 693 (2017) 462–467.
[25] J.Y. Jong, J. Zhu, S. Il Pak, G.H. Sim, Theoretical investigation of mechanical, electronic, and thermal properties of Fe2TiSi and Fe2TiSn under pressure, J. Electron. Mater. 45 (2016) 5104–5111.
[26] B.G. Yalcin, Ground state properties and thermoelectric behavior of Ru2VZ (Z=Si, ge, sn) half-metallic ferromagnetic full-Heusler compounds, J. Magn. Magn. Mater. 408 (2016) 137–146.
[27] M.W. Mohamedi, A. Chahed, A. Amar, H. Rozale, A. Lakdja, O. Benhelal, A. Sayede, Ab-initio study of structural, elastic, thermal, electronic and magnetic properties of quaternary Heusler alloys CoMnCrZ (Z = Al, As, Si, Ge), Eur. Phys. J. B. 89 (2016).
[28] M. Ahmad, Naeemullah, G. Murtaza, R. Khenata, S. Bin Omran, A. Bouhemadou, Structural, elastic, electronic, magnetic and optical properties of RbSrX(C, SI, Ge) half-Heusler compounds, J. Magn. Magn. Mater. 377 (2015) 204–210.
[29] X.R. Chen, M.M. Zhong, Y. Feng, Y. Zhou, H.K. Yuan, H. Chen, Structural, electronic, elastic, and thermodynamic properties of the spin-gapless semiconducting Mn2CoAl inverse Heusler alloy under pressure, Phys. Status Solidi Basic Res. 252 (2015) 2830–2839.
[30] M.H. Elahmar, H. Rached, D. Rached, R. Khenata, G. Murtaza, S. Bin Omran, W.K. Ahmed, Structural, mechanical, electronic and magnetic properties of a new series of quaternary Heusler alloys CoFeMnZ (Z=Si, As, Sb): a first-principle study, J. Magn. Magn. Mater. 393 (2015) 165–174.
[31] M. Benkabou, H. Rached, A. Abdellaoui, D. Rached, R. Khenata, M.H. Elahmar, B. Abidri, N. Benkhettou, S. Bin-Omran, Electronic structure and magnetic properties of quaternary Heusler alloys CoRhMnZ (Z = Al, Ga, Ge and Si) via first-principle calculations, J. Alloy. Comp. 647 (2015) 276–286.
[32] N. Mehmood, R. Ahmad, G. Murtaza, Ab initio investigations of structural, elastic, mechanical, electronic, magnetic, and optical properties of half-Heusler compounds RhCrZ (Z = Si, Ge), J. Supercond. Nov. Magn. 30 (2017) 2481–2488.
[33] S. Yousuf, D.C. Gupta, Thermoelectric and mechanical properties of gapless Zr2MnAl compound, Indian J. Phys. 91 (2017) 33–41.
[34] T. Song, J.-H. Tian, Q. Ma, X.-W. Sun, Z.-J. Liu, Electronic structure, phase stability, and elastic properties of inverse Heusler compound Mn2RuSi at high pressure, J. Supercond. Nov. Magn. 30 (2017) 951–958.
[35] A. Akriche, H. Bouafia, S. Hiadsi, B. Abidri, B. Sahli, M. Elchikh, M.A. Timaoui, B. Djebour, First-principles study of mechanical, exchange interactions and the robustness in Co2MnSi full Heusler compounds, J. Magn. Magn. Mater. 422 (2017) 13–19.
[36] P. V Sreenivasa Reddy, V. Kanchana, G. Vaitheeswaran, D.J. Singh, Predicted superconductivity of Ni 2 VAl and pressure dependence of superconductivity in Ni 2 NbX (X = Al, Ga and Sn) and Ni 2 VAl, J. Phys. Condens. Matter 28 (2016) 115703.
[37] N. Belmiloud, F. Boutaiba, A. Belabbes, M. Ferhat, F. Bechstedt, Half-Heusler compounds with a 1eV (1.7eV) direct band gap, lattice-matched to GaAs (Si), for solar cell application: a first-principles study, Phys. Status Solidi Basic Res. 253 (2016) 889–894.
[38] S. Khenchoul, A. Guibadj, B. Lagoun, A. Chadli, S. Maabed, First-Principles prediction of structural, magnetic, electronic, and elastic properties of full-Heusler compounds Co2YIn (Y = Ti, V), J. Supercond. Nov. Magn. 29 (2016) 2225–2233.
[39] M. Zemouli, A. Boudali, B. Doumi, A. Mokaddem, M. Elkeurti, F. Saadaoui, M.D. Khodja, First-Principles investigation of elastic, electronic, and half-metallic ferrimagnetic properties in the Mn 2 RhSi Heusler alloy, J. Supercond. Nov. Magn. (2016) 3187–3192.
[40] O.M. Abid, S. Menouer, A. Yakoubi, H. Khachai, S. Bin Omran, G. Murtaza, D. Prakash, R. Khenata, K.D. Verma, Structural, electronic, elastic, thermoelectric and thermodynamic properties of the NbMSb half Heusler (M=Fe, Ru, Os) compounds with first principle calculations, Superlattice. Microst. 93 (2016) 171–185.
[41] A. Boudali, M. Zemouli, F. Saadaoui, M.D. Khodja, Structural, elastic, electronic, and magnetic properties of the full-Heusler compounds Ti2NiX (X= Al, Ga, and in), J. Supercond. Nov. Magn. (2016) 1–9.
[42] C. Çoban, Y. Çiftçi, K. Çolakoğlu, Structural, electronic, elastic, optical, and vibrational properties of HfXSb (X = Co, Rh, Ru) half-Heusler compounds: an ab initio study, Indian J. Phys. 90 (2016) 1233–1241.
[43] B. Hamri, B. Abbar, A. Hamri, O. Baraka, A. Hallouche, A. Zaoui, Electronic structure and mechanical properties of X2MnSn (X = Cu, Ni, Pd) under hydrostatic pressure: GGA + U calculations, Comput. Condens. Matter. 3 (2015) 14–20.
[44] K. Bencherif, A. Yakoubi, N. Della, O. Miloud Abid, H. Khachai, R. Ahmed, R. Khenata, S. Bin Omran, S.K. Gupta, G. Murtaza, First principles investigation of the elastic, optoelectronic and thermal properties of XRuSb: (X = V, Nb, Ta) semi-Heusler compounds using the mBJ exchange potential, J. Electron. Mater. 45 (2016) 3479–3490.
[45] T. Lantri, S. Bentata, B. Bouadjemi, W. Benstaali, B. Bouhafs, A. Abbad, A. Zitouni, Effect of Coulomb interactions and Hartree-Fock exchange on structural, elastic, optoelectronic and magnetic properties of Co2MnSi Heusler: a comparative study, J. Magn. Magn. Mater. 419 (2016) 74–83.
[46] J. Li, Z. Zhang, Z. Lu, H. Xie, W. Fang, S. Li, C. Liang, F. Yin, The strain induced band gap modulation from narrow gap semiconductor to half-metal on Ti 2 CrGe: a first principles study, AIP Adv. 5 (2015) 117225.
[47] H. Lashgari, M.R. Abolhassani, A. Boochani, E. Sartipi, A. Ghaderi, Ab initio study of electronic , magnetic , elastic and optical properties of full Heusler Co 2 MnSb, Indian J. Phys. 90 (2016) 909–916.
[48] S. Amari, B. Bouhafs, Electronic, elastic, and magnetic properties of the full-Heusler with the 4d transition metal element, Co 2 YSi, Co 2 ZrSi, and Co 2 Y 0.5 Zr 0.5 Si: a first-principle study, J. Supercond. Nov. Magn. 29 (2016) 2311–2317.
[49] S. Qi, C.-H. Zhang, B. Chen, J. Shen, N. Chen, First-principles study on the ferrimagnetic half-metallic Mn2FeAs alloy, J. Solid State Chem. 225 (2015) 8–12.
[50] M.A. Hossain, T. Rahman, M. Khatun, E. Haque, Structural, elastic, electronic, magnetic and thermoelectric properties of new quaternary Heusler compounds CoZrMnX (X=Al, Ga, Ge, In), Comput. Condens. Matter. 15 (2018) 31–41.
[51] R. Ahmad, N. Mehmood, A Density Functional Theory Investigations of Half-Heusler Compounds RhVZ (Z = P, As, Sb), 2018, pp. 1577–1586.
[52] R. Ahmad, N. Mehmood, Investigation of Half-Heusler Compounds RhCrZ (Z = P, As, Sb, Sn): A First Principle Study, 2018, pp. 2637–2645.
[53] R. Ahmad, N. Mehmood, A First Principle Study of Half-Heusler Compounds CrTiZ (Z = P, As), 2018, pp. 257–264.
[54] R. Ahmad, N. Mehmood, Theoretical Investigations of Properties of New Half-Heusler Compounds NiFeZ (Z = Si, Ge), 2018, pp. 1751–1759.
[55] R. Ahmad, N. Mehmood, S. Bukhari, W. Nafees, M. Arif, Ab Initio Study of Half-Heusler Compounds MnVZ (Z = P, As, Sb), 2018, pp. 2617–2627.
[56] A. Amudhavalli, R. Rajeswarapalanichamy, K. Iyakutti, Journal of Magnetism and Magnetic Materials First principles study on Fe based ferromagnetic quaternary Heusler alloys, J. Magn. Magn. Mater. 441 (2017) 21–38.
[57] A. Amudhavalli, R. Rajeswarapalanichamy, K. Iyakutti, A.K. Kushwaha, Computational Condensed Matter First principles study of structural and optoelectronic properties of Li based half Heusler alloys, Comput. Condens. Matter. 14 (2018) 55–66.
[58] A. Bahnes, A. Boukortt, H. Abbassa, D.E. Aimouch, R. Hayn, A. Zaoui, Half-metallic ferromagnets behavior of a new quaternary Heusler alloys CoFeCrZ (Z ¼ P, As and Sb): Ab -initio study, J. Alloy. Comp. 731 (2018) 1208–1213.
[59] T.M. Bhat, D.C. Gupta, Effect of high pressure and temperature on structural , thermodynamic and thermoelectric properties of quaternary CoFeCrAl alloy, J. Electron. Mater. 47 (2018) 2042–2049.
[60] J.F.R.A.M. Blas, Investigation on the structural , elastic , electronic , and magnetic properties of half-metallic Co 2 MnSi and CoMnIrSi via first-principles calculations, J. Comput. Electron. 17 (2018) 1470–1477.
[61] A. Candan, S. Akbudak, M. Özduran, A. İyigör, An examination of the structural , electronic , elastic , vibrational and thermodynamic properties of Ru 2 YGa (Y = Sc , Ti and V) Heusler alloys, Chinese J. Phys. 56 (2018) 1772–1780.
[62] M. Chehrouri, B. Doumi, A. Mokaddem, Y. Mogulkoc, Investigation of structural stability , elastic properties, electronic structure and ferrimagnetic behavior of Mn 2 RhGe full-Heusler alloy, J. Alloy. Comp. 722 (2017) 564–568.
[63] S. Chibani, O. Arbouche, M. Zemouli, Y. Benallou, K. Amara, N. Chami, M. Ameri, M. El Keurti, Computational Condensed Matter First-principles investigation of structural , mechanical , electronic , and thermoelectric properties of Half-Heusler compounds RuVX (X ¼ As , P , and Sb), Comput. Condens. Matter. 16 (2018), e00312.
[64] B. Fadila, M. Ameri, D. Bensaid, M. Noureddine, I. Ameri, S. Mesbah, Y. Al-douri, Journal of Magnetism and Magnetic Materials Structural , magnetic , electronic and mechanical properties of full-Heusler alloys Co 2 YAl (Y = Fe , Ti): first principles

calculations with different exchange-correlation potentials, J. Magn. Magn. Mater. 448 (2018) 208–220.
[65] Y. Guermit, M. Drief, N. Benkhettou, T. Lantri, B. Abidri, D. Rached, Phase stability , electronic , magnetic and elastic properties of Ni 2 Co Z (Z = Ga , Sn): a first principles study with GGA method and GGA + U approach, Chin. J. Phys. 56 (2018) 1394–1404.
[66] Y. Han, Y. Wu, T. Li, R. Khenata, T. Yang, X. Wang, Properties of a New Equiatomic Quaternary Heusler Compound YRhTiGe , A First-Principles Study, 2018.
[67] E. Haque, M.A. Hossain, Thermoelectric transport properties of TaCoSn, Results Phys. 10 (2018) 458–465.
[68] H.M. Huang, S.J. Luo, Y.C. Xiong, Properties of half-Heusler compound CoCrBi, J. Magn. Magn. Mater. 438 (2017) 5–11.
[69] R. Jain, V. Kumar, J. Aarti, R.C. Vishal, J.N. Lakshmi, Study of the electronic structure , magnetic and elastic properties and half-metallic stability on variation of lattice constants for CoFeCrZ (Z = P, As, Sb) Heusler Alloys, J. Supercond. Nov. Magn. (2018) 2399–2409.
[70] D. Jiang, Y. Ye, Q. Gou, D. Wu, Y. Wen, First-principles predictions on structural , elastic and half-metallic properties of Fe 2 LiAs Heusler compound, J. Magn. Magn. Mater. 458 (2018) 235–240.
[71] X. Kang, J. Zhang, The structural , electronic , elastic , thermodynamic , magnetic , and optical properties of the yttrium-based full-Heusler alloys Y 2 CrZ (Z ¼ Si, Ge, Sn), J. Phys. Chem. Solids 119 (2018) 71–79.
[72] F. Khelfaoui, M. Ameri, D. Bensaid, I.A.Y. Al-douri, Structural , Elastic , Thermodynamic , Electronic , and Magnetic Investigations of Full-Heusler Compound Ag 2 CeAl : FP-LAPW Method, 2018, pp. 3183–3192.
[73] A. Kundu, S. Ghosh, Intermetallics First principles study of the structural phase stability and magnetic order in various structural phases of Mn 2 FeGa, Intermetallics 93 (2018) 209–216.
[74] S. Lee, Robust mechanical stability , electronic structure , magnetism and thermoelectric properties of CoFeMnSb quaternary Heusler alloy: a fi rst principle study, J. Alloy. Comp. 742 (2018) 903–909.
[75] L. Liu, X. Wu, R. Wang, H. Mao, Y. Jiang, Y. He, Y. Wen, First-Principle Calculations on the Structural , Mechanical , and Electronic Properties of Mn 2 RuSi and Mn 2 RuGe under Pressure, 2018, pp. 3667–3677.
[76] L. Liu, X. Zeng, Q. Gou, Y. Ye, The Structural Stability and Mechanical Properties of Cu 2 MnAl and Cu 2 MnIn under Pressure: First-Principles Study, 2018, p. 47.
[77] N. Mehmood, R. Ahmad, Structural , Electronic , Magnetic and Optical Investigations of Half-Heusler Compounds YZSb (Z = Cr , Mn), FP-LAPW Method, 2018, pp. 879–888.
[78] D. Mokhtari, H. Baaziz, D. Guendouz, Z. Charifi, B. Hamad, Theoretical Investigation of Structural , Electronic , Magnetic , and Mechanical Properties of Quaternary Heusler Alloys CoVTiX (X = as , Si), 2018, pp. 3625–3636.
[79] E.G. Özdemir, E. Eser, Z. Merdan, Investigation of structural , half-metallic and elastic properties of a new full-Heusler compound – Ir 2 MnSi, Chin. J. Phys. 56 (2018) 1551–1558.
[80] P.D. Patel, S. Shinde, S.D. Gupta, S.D. Dabhi, P.K. Jha, The first principle calculation of structural, electronic , magnetic , elastic , thermal and lattice dynamical properties of fully compensated ferrimagnetic spin-gapless Heusler alloy Zr 2 MnGa, Comput. Condens. Matter. 15 (2018) 61–68.
[81] F.A. Polymorphs, M. Friák, S. Oweisová, J. Pavl, D. Holec, An Ab Initio Study of Thermodynamic and Mechanical Stability of Heusler-Based, (n.d.).
[82] D. Rani, K.G. Suresh, A.K. Yadav, D. Bhattacharyya, M.R. Varma, A. Alam, Structural, electronic, magnetic and transport properties of equiatomic quaternary Heusler alloy CoRhMnGe: theory and experiment, Phys. Rev. B (2018) 1–11.
[83] V.A. Shukoor, M. Sarwan, S. Singh, High pressure structural, elastic and electronic properties of a new half Heusler compound: AuYPb, Phys. B Phys. Condens. Matter. 547 (2018) 83–87.
[84] L. Siakeng, M. Mikhailov, D.P. Rai, Compounds Co 2 FeAl and Fe 2 CoAl , Promising Materials for Spintronic Applications : a DFT + U Approach, 2018, pp. 10341–10349.
[85] J. Wang, Z.B. Chen, Y.C. Gao, Phase stability , magnetic , electronic , half-metallic and mechanical properties of a new equiatomic quaternary Heusler compound ZrRhTiIn : a fi rst-principles investigation, J. Phys. Chem. Solids 116 (2018) 72–78.
[86] X. Wang, Z. Cheng, G. Liu, X. Dai, L. Wang, A. Bouhemadou, Rare Earth-Based Quaternary Heusler Compounds, 2017, pp. 1–12.
[87] X. Wang, H. Khachai, R. Khenata, H. Yuan, L. Wang, W. Wang, A. Bouhemadou, L. Hao, X. Dai, R. Guo, Structural , electronic , magnetic , half-metallic , mechanical , and thermodynamic properties of the quaternary Heusler compound FeCrRuSi : a first-principles study, Sci. Rep. (2017) 1.
[88] X. Wang, W. Zhao, Z. Cheng, X. Dai, R. Khenata, Electronic , magnetic , half-metallic and mechanical properties of a new quaternary Heusler compound ZrRhTiTl : insights from fi rst-principles studies, Solid State Commun. 269 (2018) 125–130.
[89] S. Yousuf, D.C. Gupta, Investigation of spin polarized band structure , magnetism , and mechanical properties of new gapless Zr 2 NbX (X ¼ Al , Ga , in) Heusler alloys, J. Alloy. Comp. 766 (2018) 241–247.
[90] S. Yousuf, D.C. Gupta, Chemical potential evaluation of thermoelectric and mechanical properties of Zr 2 CoZ (Z = Si , Ge) Heusler alloys, J. Electron. Mater. 47 (2018) 2468–2478.
[91] J. Zhao, Q. Gao, L. Li, H. Xie, X. Hu, C. Xu, Intermetallics First-principles study of the structure , electronic , magnetic and elastic properties of half-Heusler compounds LiXGe (X = Ca , Sr and Ba), Intermetallics 89 (2017) 65–73.
[92] S. Dergal, B. Doumi, A. Mokaddem, S. Mamoun, A.E. Merad, A novel theoretical prediction of electronic structure, phase stability, and half-metallic ferromagnetic behavior of new quaternary RhFeTiZ (Z = Al, Si) Heusler alloys, J. Supercond. Nov. Magn. 29 (2016) 2953–2959.
[93] S.F. Pugh, XCII. Relations between the elastic moduli and the plastic properties of polycrystalline pure metals, Lond. Edinb. Dublin Philos. Mag. J. Sci. 45 (1954) 823–843.
[94] L. Pauling, General Chemistry, third ed., Dover Publications, 1970.
[95] P.R. Strutt, R.S. Polvani, J.C. Ingram, Creep behavior of the Heusler type structure alloy Ni2AlTi, Metall. Trans. A. 7 (1976) 23–31.